ACS OMEGA

http://pubs.acs.org/journal/acsodf

Article

Medium Bandgap Nonfullerene Acceptor for Efficient Ternary Polymer Solar Cells with High Open-Circuit Voltage

Mukhamed L. Keshtov,* Alexei R. Khokhlov, Dimitriy Y. Shikin, Vladimir Alekseev, Giriraj Chayal, Hemraj Dahiya, Manish Kumar Singh, Fang Chung Chen, and Ganesh D. Sharma*

Cite This: *ACS Omega* 2023, 8, 1989−2000

Read Online

ACCESS | Metrics & More | Article Recommendations | Supporting Information

ABSTRACT: We have designed a new medium bandgap non-fullerene small-molecule acceptor consisting of an IDT donor core flanked with 2-(6-oxo-5,6-dihydro-4*H*-cyclopenta[*c*]-thiophene-4-ylidene) malononitrile (TC) acceptor terminal groups (**IDT-TC**) and compared its optical and electrochemical properties with the IDT-IC acceptor. **IDT-TC** showed an absorption profile from 300 to 760 nm, and it has an optical bandgap of 1.65 eV and HOMO and LUMO energy levels of −5.55 and −3.83 eV, respectively. In contrast to IDT-IC, **IDT-TC** has an upshifted LUMO energy level, which is advantageous for achieving high open-circuit voltage. Moreover, **IDT-TC** showed higher crystallinity and high electron mobility than IDT-IC. Using a wide bandgap D−A copolymer P as the donor, we compared the photovoltaic performance of **IDT-TC**, IDT-IC, and IDT-IC-Cl nonfullerene acceptors (NFAs). Polymer solar cells (PSCs) using P: **IDT-TC**, P: IDT-IC, and P:IDT-IC-Cl active layers achieved a power conversion efficiency (PCE) of 14.26, 11.56, and 13.34%, respectively. As the absorption profiles of IDT-IC-Cl and **IDT-TC** are complementary to each other, we have incorporated **IDT-TC** as the guest acceptor in the P: IDT-IC-Cl active layer to fabricate the ternary (P:**IDT-TC**: IDT-IC-Cl) PSC, demonstrating a PCE of 16.44%, which is significantly higher than that of the binary BHJ devices. The improvement in PCE for ternary PSCs is attributed to the efficient exploitation of excitons via energy transfer from **IDT-TC** to IDT-IC-Cl, suitable nanoscale phase separation, compact stacking distance, and more evenly distributed charge transport.

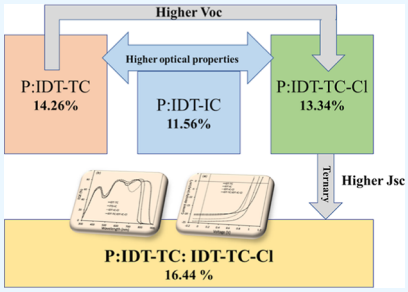

1. INTRODUCTION

The polymer solar cells (PSCs) are seen to be promising after developing the concept of bulk heterojunction (BHJ)[1] due to their low cost and large area, semitransparent nature, and environmentally friendly photovoltaic technology using solution-processed roll-to-roll printing techniques.[2−8] The development of the novel Y6 small-molecule acceptor (SMA), reported by Zou et al., in 2019, realized a power conversion efficiency (PCE) of 15.7% for PSCs.[9] An improved PCE of 15.98% has been achieved using modified Y6, that is, N3 SMA,[10] and recently, over 17% of as-cast PSCs have also been reported.[11] Currently, the PCE of PSCs has reached 18−19% for the single junction PSCs based on narrow bandgap SMAs via the use of additives and interface engineering.[12−16]

Furthermore, besides the narrow bandgap SMAs, medium bandgap SMAs (i.e., optical bandgap in the range 1.6−1.8 eV) have also been designed and used considerably for PSCs.[17−25] The photons below the wavelength range of 300−800 nm may be fully harvested by the PSCs, which are made of a medium bandgap SMA and a wide bandgap polymer donor. A high open-circuit voltage (V_{OC}) produced by SMAs' upshifted LUMO energy level makes them the ideal front subcells for tandem solar cells.[26−29] In order to achieve a PCE of 10.08% with a high V_{OC} of 0.98 V, Chen et al. created a medium bandgap SMA F-M with an optical bandgap of 1.65 eV and employed it as an acceptor along with copolymer donor PBDB-T.[30] When the PBDB-T: F-M active layer was used in the front subcell, the tandem solar cells realized a record PCE of 17.36%.[31] Ding et al. have synthesized a medium bandgap SMA, IBCT, which exhibits a bandgap of 1.65 eV. In order to achieve an overall PCE of 11.26% with a high V_{OC} of 1.02 V, the medium bandgap IBCT is used as an acceptor together with a wide bandgap polymer L1. In tandem solar cells, they have also employed the L1:IBCT active layer as the front subcell and have attained a PCE of 15.25%.[32] A PCE of 18.71% was obtained by Huang et al. using a medium bandgap SMA in the front cell of the tandem PSCs.[33] While using a wide bandgap polymer donor and narrow bandgap SMA, the binary BHJ active layer only absorbs photons in the shorter and longer wavelength regions, thereby limiting PSCs' light-harvesting ability and also the value of J_{SC} of the PSCs.[34] To broaden the absorption profile from 300 to 900 nm and improve the exciton generation and morphology of the BHJ

Received: August 10, 2022
Accepted: November 8, 2022
Published: January 2, 2023

Chart 1. Chemical Structure of IDT-TC, IDT-IC, IDT-IC-Cl, and P

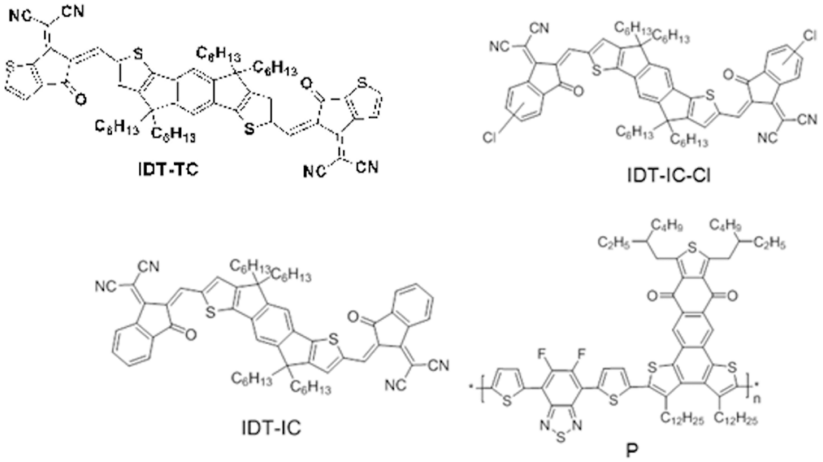

Scheme 1. Synthesis Route for IDT-TC

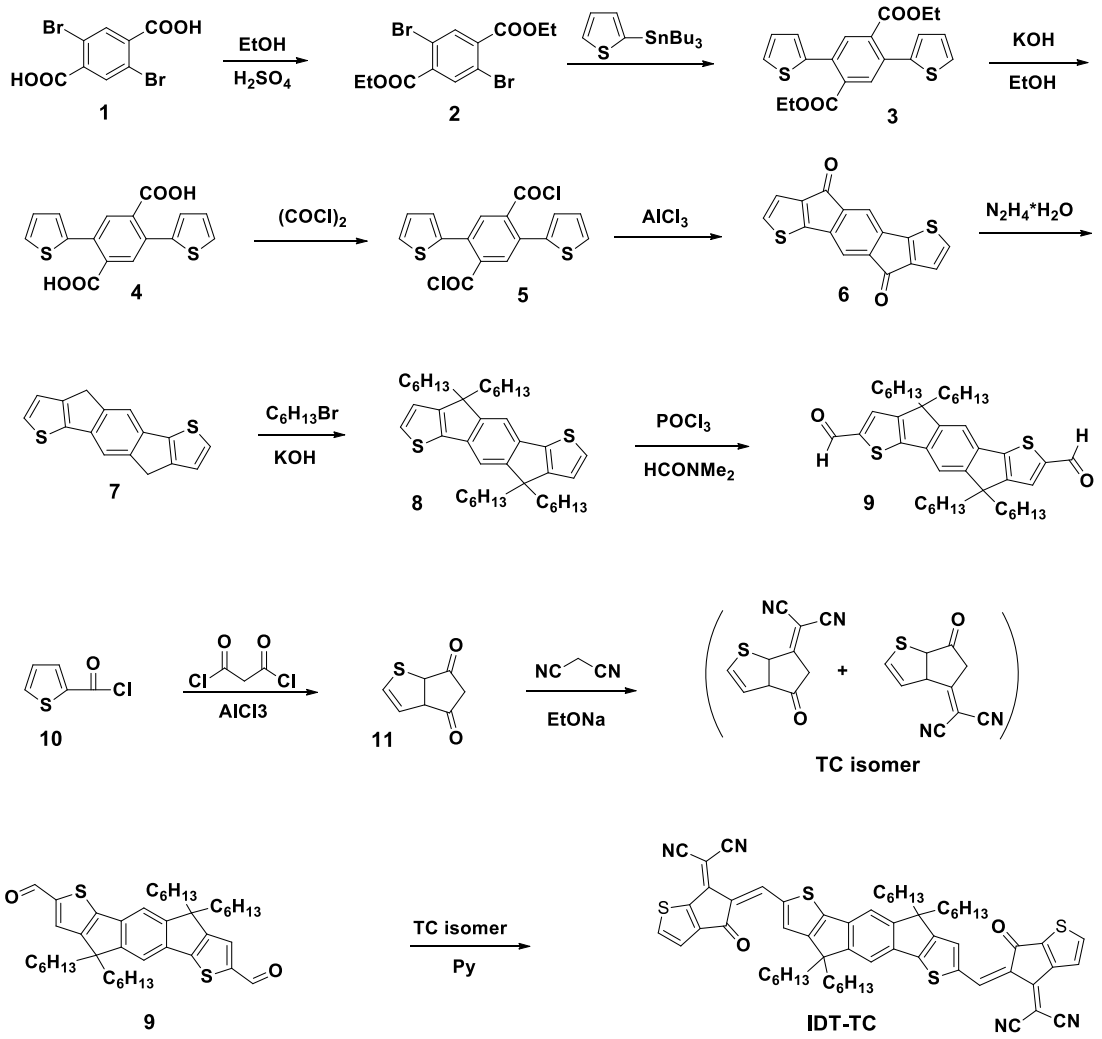

active layer, the ternary concept has been developed by incorporating either a second acceptor or donor as a guest component material into the host binary BHJ active layer.[35−39] This notion is useful for optimizing the light-harvesting, exciton dissociation, and charge transport in the active ternary layers.[40] Furthermore, ternary PSCs retain the simple fabrication technique utilized for binary BHJ PSCs and alter the energy level matching of the D/A interface, which is also required to achieve a high PCE. The addition of a third material to a ternary BHJ active layer can raise the V_{OC}, expand the absorption profile, and improve photon harvesting, all of which increase the short-circuit current (J_{SC}). Additionally, the fill factor (FF) of the PSCs is improved, and the charge carrier transit is improved by an appropriate cascade energy level

https://doi.org/10.1021/acsomega.2c05141
ACS Omega 2023, 8, 1989−2000

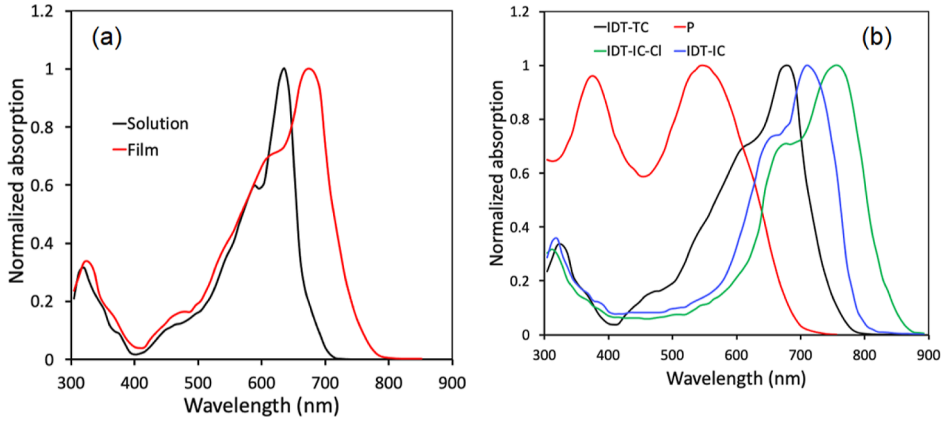

Figure 1. Normalized absorption spectra of **IDT-IC** in (a) dilute solution and film and (b) thin absorption spectra of **IDT-TC**, IDT-IC, IDT-IC-Cl, and P.

structure, which also suppresses the recombination processes.[24] In some cases, the third component can act as an additional energy donor by forming an efficient energy transfer channel with the host binary system and improving the efficiency of photogenerated exciton generation.[41−43] This occurs when the third component's PL spectrum overlaps with the host's (donor or acceptor) absorption spectra.

In order to create high-performing SMAs, terminal group engineering is essential. The LUMO levels of A-D-A SMAs and, consequently, the V_{OC} values can be significantly influenced by terminal units according to predictions made by researchers.[44−47] Additionally, since the molecular packing of A-D-A SMAs is mostly dependent on the terminal group stacking, tightly packed end-groups speed up the electron transport. 2-(6-Oxo-5,6-dihydro-4*H*-cyclopenta[*c*]-thiophene-4-ylidene)malononitrile denoted as TC is a potential end-group for the designing of A−D−A acceptors due to its strong light harvesting from the electron delocalization and reasonable charge transport originating from the strong intermolecular S−S interactions.[48,49] Zou et al. have created an A-DA′D−A NFA Y10 consisting of a weak TPBT-based core and two electron-accepting units of TC, and the PSCs based on this non-fullerene acceptor (NFA) demonstrate a PCE of 13.46%.[50] Xie et al. designed an NFA of ITCPTC with the thiophene fused ending group and achieved a PCE of 11.8% with an FF of 0.751, which is 20% higher than for the ITIC-based counterpart.[51] An outstanding V_{OC} of 1.10 V and an efficiency of about 7.34% were attained by Gao et al. when they combined the donor, a conjugated polymer PBDB-T, with a twisted NFA acceptor with thiophene fused terminal groups.[52]

A novel A−D−A SMA, designated **IDT-TC**, has been created and synthesized using an IDT donor core and TC acceptor terminals. **IDT-TC** displayed an absorption profile between 300 and 760 nm (optical bandgap of 1.65 eV) with HOMO/LUMO energy levels of −5.55/−3.83 eV. We have compared the photovoltaic performance of **IDT-TC** with two other non-fullerenes having the same donor core as **IDT-TC** with different terminal units, that is, IDT-IC and IDT-IC-Cl.[53] The high-lying LUMO of **IDT-TC** is beneficial for attaining V_{OC} for the PSCs. We have used a wide bandgap D−A1−D−A2 conjugated polymer P as a donor with donor thiophene (D) and fluorinated benzothiadiazole (A1) and anthra[1,2-*b*:4,3,*b*′:6,7-*c*″]trithiophene-8.12-dione (A2).[54] In Chart 1, the chemical structures of **IDT-TC**, IDT-IC, IDT-IC-Cl, and P are shown. Our fabrication of binary BHJ PSCs resulted in a greater overall PCE of 14.26% with a V_{OC} of 1.04 V than the PSC based on the IDT-IC equivalent (12.15%). Using P as the donor and narrow bandgap IDT-IC-Cl as the acceptor, we also designed PSCs, achieving an overall PCE of 13.35% with a V_{OC} of 0.86 V. In order to create the ternary (P:**IDT-TC**: IDT-IC-Cl) PSCs, we added a little amount of **IDT-TC** as a third component to the binary P: IDT-IC-Cl. We obtained a PCE of 16.44% with a V_{OC} of 0.96 V.

2. EXPERIMENTAL SECTION

2.1. Materials. All of the reagents and chemicals were purchased from Aldrich, Acros, TCI and used without further purification. Toluene was dried and purified by fractional distillation over sodium/benzophenone under argon. The intermediate compounds and their characterizations are described in Supporting Information.

2.2. Synthesis of 2,2′-((5Z,5′Z)-5,5′-((4,4,9,9-Tetrahexyl-4,9-dihydro-*s*-indaceno[1,2-*b*:5,6-*b*′]dithiophene-2,7-diyl)*bis*(methanylylidene))*bis*(6-oxo-5,6-dihydro-4*H*-cyclopenta[*b*]thiophene-5,4-diylidene))-dimalononitrile (IDT-TC). The synthesis of **IDT-TC** is shown in Scheme 1. Pyridine (1.3 mL) was added to a solution of dialdehyde 9 (0.13, 0.2 mmol) and indanon TC (0.40 g, 0.4 mol) in chloroform (65 mL) in an argon atmosphere, and then, the mixture was boiled for 25 h. After cooling to room temperature, the mixture was poured into methanol, and the precipitate was filtered and purified by column chromatography using hexane/dichloromethane (1:1.2/v) as an eluent. The yield of the target product is 102 mg, 50%. ^{1}H NMR (500 MHz $CDCl_3$) (Figures S1 and S2): δ (ppm) 8.75(s),89.74(s)-2H; 7.99 (AB), 7.90(d), 7.47(d)-4H; 7.68(s)-2H; 7.58(s)-2H; 2.20−1.90 (8H); 1.30−1/00(24H);9.95−0.65(2H). ^{13}CNMR (100 MHz, $CDCl_3$): δ (ppm) 182.45, 180.77, 158.78, 157.44, 156.98, 156.19, 152.44, 152.27, 150.19, 148.45, 139.91, 139.24, 137.67, 136.92, 136.53, 124.53, 124.18, 123.56, 121.29, 115.69, 114.46, 114.37, 114.01, 113.79, 68.91, 67.31, 54.30,39.09, 31.53, 29.56.24.32,22.56, 13.99. Elem. Anal. Calcd for $C_{62}H_{62}N_4O_2S_4$: C, 72.76; H, 6.11; N, 5.47; S, 12.53. Found: C, 72.49; H, 6.00; N, 5.29; S, 12.21%.

2.3. Device Fabrication and Characterization. The PSCs with the structure of ITO/PEODT/PSS/active layer/PFN/Al were fabricated to evaluate the photovoltaic performance of **IDT-TC**, IDT-IC, and IDT-IC-Cl as acceptors and P

https://doi.org/10.1021/acsomega.2c05141
ACS Omega 2023, 8, 1989−2000

Table 1. Thermal, Optical, and Electrochemical Properties of IDT-IC

acceptor	$T_{5\%}$ [°C]	λ_{max} (sol) [nm]	λ_{max} (film) [nm]	E_{HOMO} [eV]	E_{LUMO} [eV]	E_g^{ech} [eV]	E_g^{opt} [eV]
IDT-TC	342	635 (2.3×10^5 M^{-1} cm^{-1})[a]	674	−5.57	−3.81	1.73	1.65

[a]Molar extinction coefficient.

as the donor. The detailed fabrication of PSCs is described in Supporting Information.

3. RESULTS AND DISCUSSION

3.1. Synthesis and Characterization of IDT-TC. Scheme 1 describes the synthesis process of **IDT-TC**. Experimental details to synthesize the intermediate compounds are described in the Supporting Information. The target NFA 2,2′-((5Z,5′Z)-5,5′-((4,4,9,9-tetrahexyl-4,9-dihydro-*s*-indaceno[1,2-*b*:5,6-*b*′] dithiophene-2,7-diyl)*bis*(methanylylidene))*bis*(6-oxo-5,6-dihydro-4*H*-cyclopenta[*b*]thiophene-5,4-diylidene))-dimalononitrile (**IDT-TC**) was synthesized through the Knoevenagel condensation reaction between dialdehyde **9** and TC with 50% yield. ^{1}H NMR confirmed the composition and structure of all intermediates. The target product (**IDT-TC**) was characterized by ^{1}H NMR, ^{13}C NMR, and elemental analysis (Figures S1 and S2, Supporting Information). The elemental analysis is also summarized in the Supporting Information.

At room temperature, **IDT-TC** is highly soluble in common organic solvents like chloroform, toluene, and o-dichlorobenzene. With a breakdown temperature (T_d, 5% weight loss) of 342 °C (Figure S3, Supporting Information), **IDT-TC** demonstrates outstanding thermal stability, which is advantageous for optoelectronic devices.

3.2. Optical and Electrochemical Properties. Figure 1a displays the normalized absorption spectra in a thin-film cast and diluted chloroform solution, and related results are reported in Table 1. **IDT-TC** displayed two distinct absorption bands in both solution and film, namely, 300−400 nm for the $\pi-\pi^*$ transition[55] and 400−750 nm for the intramolecular charge transfer (ICT) between the central donor core and terminal acceptor units. The ICT peak in the thin-film absorption spectra is red-shifted (42 nm) in comparison to that in the solution, showing strong molecular backbone aggregations and—interactions in the solid state. The optical bandgap estimated from the onset of thin-film absorption spectra was about 1.65 eV. Figure 1b also displays the thin-film absorption spectra for IDT-IC, IDT-IC-Cl, and P. The absorption of **IDT-TC**, IDT-IC, and IDT-IC-Cl was complimentary to that of P, which is advantageous for a high value of J_{SC} of the resultant PSCs via increasing the photon harvesting range from 300 to 900 nm for the ternary active layer.

The HOMO and LUMO energy levels of **IDT-TC** were calculated via the electrochemical cyclic voltammetry (CV) technique, with $Ag/AgNO_3$ as the reference electrode and FC/Fc^+ couple as the internal reference (Figure 2). The CV curves for IDT-IC and IDT-IC-Cl are also shown in Figure S4 (Supporting Information). The measured E_{HOMO}/E_{LUMO} values of **IDT-TC** are −5.57 and −3.82 eV, respectively, whereas the E_{HOMO}/E_{LUMO} values of IDT-IC are about −5.60 and −3.94 eV, respectively.[53] We observed that with the change in the terminal unit from IC to TC, the NFA's LUMO energy level shifted up, while the HOMO energy levels remained almost unchanged. It has already been reported that the central donor unit mainly determines the HOMO of the

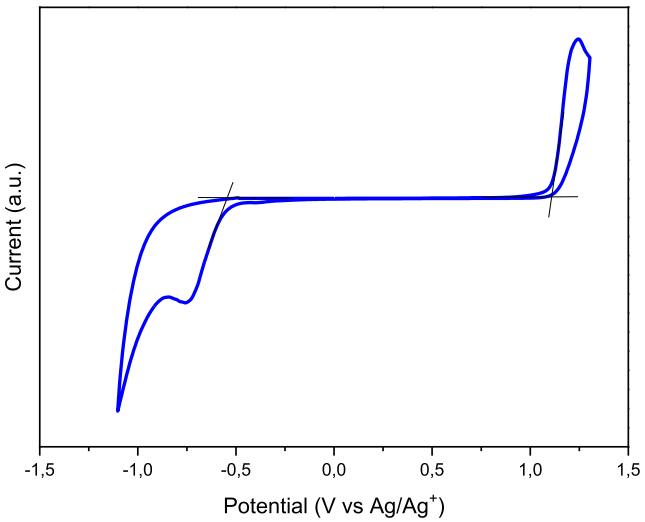

Figure 2. CV curve for **IDT-TC**.

A−D−A materials, and LUMO mainly depends upon the terminal acceptor unit. **IDT-TC** displayed blue-shifted absorption and an increased LUMO energy level in comparison to IDT-IC because thiophene has a weaker ability to donate electrons than phenyl, which reduces the ability of terminal units to withdraw electrons. This reduces the strength of the ICT effect and increases the HOMO of the resulting acceptor molecule.[56,57] The IDT-high IC's LUMO energy promotes the achievement of a greater open-circuit voltage.

3.3. Theoretical Simulations. To carry out the DFT calculation, computer models of **IDT-TC** and IDT-IC molecules were created, in which methyl ones replaced hexyl radicals. The geometry of these models in the equilibrium and transition states was estimated by the DFT/ωB97X-D3(BJ)/6-31G(d,p)++ method. Figures S5 and S6 (Supporting Information) demonstrate these findings. The models have an almost planar structure, the stability of which is ensured by forming intramolecular aromatic hydrogen bonds. HOMO and LUMO energies, HOMO and LUMO surfaces, and electrostatic potential were calculated using the DFT/MN15-L/6-31G(d,p)++ method (Figure 3 and Table 2). For both models,

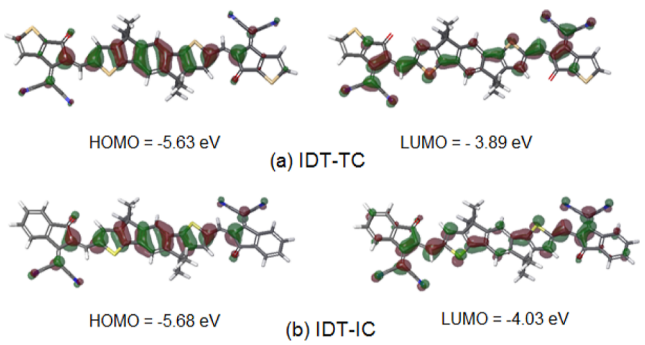

Figure 3. Molecular orbital surfaces of (a) **IDT-TC** and (b) IDT-IC calculated by the DFT/MN15-L/6-31G(d,p)++ method.

https://doi.org/10.1021/acsomega.2c05141
ACS Omega 2023, 8, 1989−2000

Table 2. HOMO and LUMO Energy Levels of IDT-TC and IDT-IC

material	HOMO (eV)	LUMO (eV)	E_g (eV)
IDT-TC, experimental data	−5.56	−3.82	1.74
IDT-TC, calculation by the DFT/MN15-L/6-31G(d,p)++ method	−5.63	−3.89	1.74
IDT-IC, calculation by the DFT/MN15-L/6-31G(d,p)++ method	−5.68	−4.03	1.65

the HOMO surfaces are located on the fragment 4,9-dihydro-*s*-indaceno[1,2-*b*:5,6-*b*′]dithiophene; the HOMO values for both models are close. LUMO surfaces are also located on the side fragments—2-(2-methylene-3-oxo-2,3-dihydro-1*H*-inden-1-ylidene)malononitrile (IC) in the case of IDT-IC and 2-(5-methylene-6-oxo-5,6-dihydro-4*H*-cyclopenta[*b*]-thiophen-4-ylidene)malononitrile (TC) in the case of **IDT-TC**. For **IDT-TC**, the LUMO value is higher, and the E_g value is greater than for IDT-IC. The negative values of the electrostatic potential are concentrated on the nitrogen atoms of the nitrile groups and the oxygen atoms of the carbonyl groups (Figure 4).

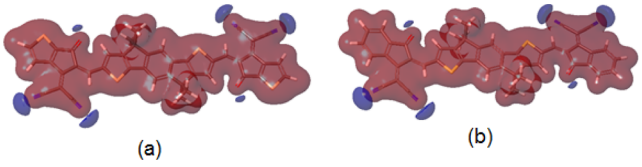

Figure 4. Electrostatic potential surface for (a) **IDT-TC** and (b) IDT-IC calculated by the DFT/M15-L/6-31(d,p)++ method.

3.4. Mobility and Crystallinity. The electron mobilities of the pristine films made with **IDT-TC** and IDT-IC were also measured (Figure S7), and it was observed that **IDT-TC** had greater electron mobility (4.78×10^{-4} cm^2/Vs) than IDT-IC (3.97×10^{-4} cm^2/Vs). This difference is most likely attributable to better electron delocalization and stronger intermolecular forces through the formation of noncovalent S−S bonds, which facilitate electron transport.

We also compared the molecular ordering and crystallinity of **IDT-TC** with those of IDT-IC via the XRD patterns (Figure S8). It can be seen from this figure that both (100) and (010) correspond to lamellar stacking, and $\pi-\pi$ stacking of **IDT-TC** was more substantial and sharper than that of IDT-IC, indicating a stronger crystallinity of **IDT-TC**. The enhancement of molecule crystallinity is beneficial for charge carrier mobility.

3.5. Photovoltaic Properties. We used the medium bandgap SMA **IDT-TC** as an acceptor and wide bandgap copolymer P as a donor to fabricate the binary BHJ PSCs. We also fabricated the PSCs using IDT-IC and IDT-IC-Cl as acceptors for comparison. In order to fabricate the ternary PSCs, we have incorporated **IDT-TC** as the second acceptor in the host P: IDT-IC-Cl binary BHJ active layer. The absorption spectra for **IDT-TC**, IDT-IC, IDT-IC-Cl, and P are shown in Figure 1b. These energy levels are shown in Figures 5 and 4b, respectively. The LUMO offsets [$\Delta E_{\mathrm{LUMO\ (D/A)}}$] for P/**IDT-IC** and P/IDT-IC-Cl are 0.23 and 0.38 eV, respectively. Figure S9 shows the photoluminescence (PL) spectra of pure P and its blend with either **IDT-TC** or IDT-IC-Cl in order to provide information regarding the electron transport from P to either of these materials. When excited at 540 nm, P displayed a

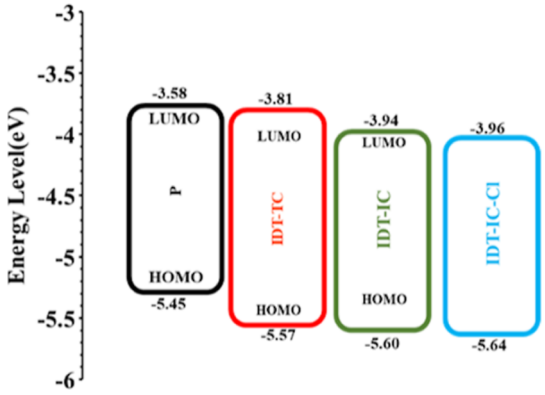

Figure 5. Energy level diagrams of **IDT-TC**, IDT-IC, IDT-IC-Cl, and P.

significant PL peak at 698 nm, which was totally quenched for both P: **IDT-TC** and P: IDT-IC-Cl, suggesting efficient electron transport from P to either **IDT-TC** or IDT-IC-Cl in their respective D/A interfaces. The HOMO offsets [$\Delta E_{\mathrm{HOMO\ (D/A)}}$] for **IDT-TC**/P and IDT-IC-Cl/P were 0.12 and 0.19 eV, respectively. As shown in Figure 6, we further

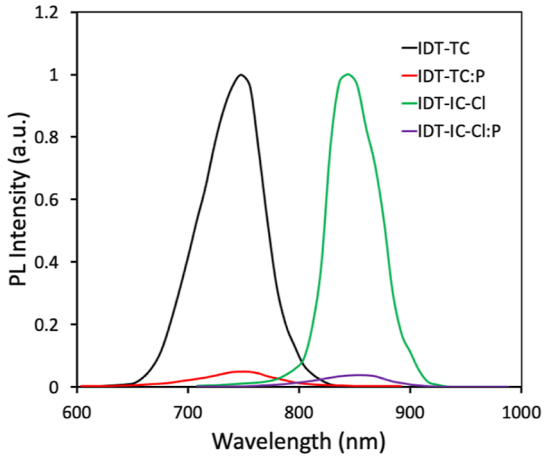

Figure 6. Thin-film PL spectra of pristine acceptors (**IDT-TC** and IDT-IC-Cl) and their blends with P.

investigated the PL spectra of pristine **IDT-TC** and IDT-IC-Cl as well as their P blends. The pristine **IDT-TC** and IDT-IC-Cl films showed strong PL peaks at 748 and 844 nm, respectively, when excited at their maximum absorption peak, which was completely quenched for their blends with P (the PL quenching efficiencies for IDT-IC:P and IDT-IC-Cl:P are about 92 and 95%), demonstrating efficient hole transfer from either **IDT-TC** or IDT-IC-Cl to P in their respective D/A interfaces, even the small $\Delta E_{\mathrm{HOMO\ (D/A)}}$, and this is observed in most of the non-fullerene PSCs.[58−60]

We have fabricated binary BHJ PSCs using P as the donor and **IDT-TC**, IDT-IC, and IDT-IC-Cl as the acceptors. By changing the weight ratio between the donor and acceptor, the photovoltaic performance was optimized. We observed that the PSCs with the best PCE had a D/A weight ratio of 1:1.2 (Table S1a−c, Supporting Information). The optimized PSC (1:1.2) was then treated with THF for 40 s in order to undergo solvent vapor annealing treatment (Table S2a−c, Supporting Information). Figure 7a shows the current−voltage character-

https://doi.org/10.1021/acsomega.2c05141
ACS Omega 2023, 8, 1989−2000

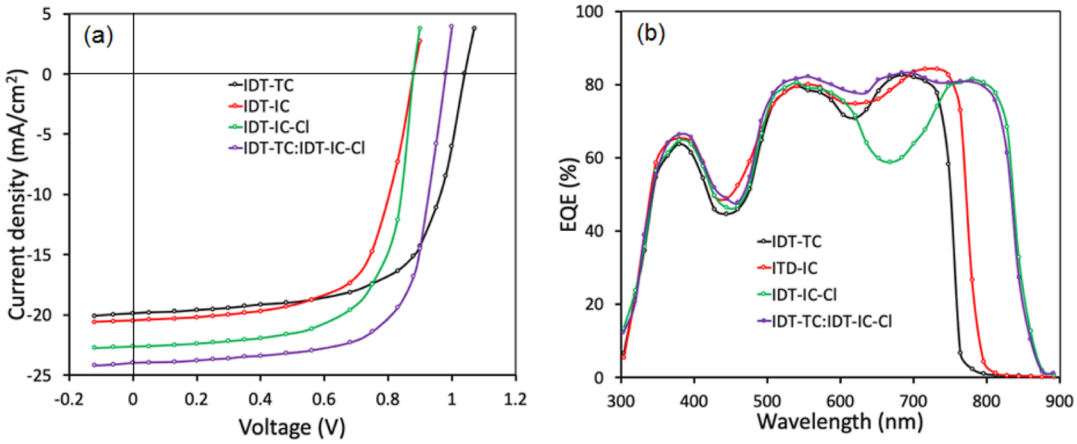

Figure 7. (a) $J-V$ characteristics under illumination (AM1.5 G, 100 mW cm^{-2}) and (b) EQE spectra of the binary and ternary PSCs.

Table 3. Photovoltaic Data for the Binary and Ternary PSCs

active layer	J_{SC} (mA/cm^2)	V_{OC} (V)	FF	PCE (%)
P:**IDT-TC (1:1.2)**	19.88 (±0.21) (19.74)[a]	1.04	0.69 (±0.014)	14.26 (±0.11) (14.14)[b]
P:IDT-IC (1:1.2)	20.52 (±0.13) (20.41)[a]	0.88	0.64 (±0.012)	11.56 (±0.14) (11.41)[b]
P:IDT-IC-Cl (1:1.2)	22.64 (±0.11) (20.52)[a]	0.88	0.67 (±0.011)	13.34 (±0.11) (13.21)[b]
P:**IDT-TC**:IDT-IC-Cl (1:0.3:0.9)	23.98 (±0.14) (23.83)[a]	0.96	0.714 (±0.015)	16.44 (±0.15) (16.21)[b]

[a]J_{SC} value estimated from EQE spectra. [b]Average of eight identical devices.

istics of optimized PSCs under illumination (AM1.5 G, 100 mW/cm^2), and Table 3 compiles associated photovoltaic data.

Although the value of J_{SC} is lowest for IDT-IC-based devices, the optimized binary BHJ PSCs based on **IDT-TC** showed a higher PCE of 14.26% to IDT-IC (11.56%) and IDT-IC-Cl (13.34%). This is because of the high values of V_{OC} and FF. As the V_{OC} is directly related to the energy difference between the HOMO of the donor and LUMO of the acceptor used in the BHJ active layer, the highest value of V_{OC} for **IDT-TC** may be associated with its high-lying LUMO energy level as compared to either IDT-IC or IDT-IC-Cl. We recorded the PSCs' external quantum efficiency (EQE) spectra in order to learn more about the variation in J_{SC} values, as depicted in Figure 7b. For **IDT-TC**, IDT-IC, and IDT-IC-Cl-based devices, respectively, the J_{SC} values derived from the integration of EQE spectra are 19.72, 20.39, and 22.47 mA/cm^2.

3.6. Ternary Polymer Solar Cells. It is reported that the ternary approach has been the efficient method to improve the PCE of PSCs owing to enhanced light harvesting ability via energy transfer from the guest component to the host system[60] and attained a PCE exceeding 19%.[12,13] Various working principles such as charge transfer, energy transfer, and alloy model have been utilized to understand the enhancement in the PCE of ternary PSCs as compared to that of the binary counterpart.[61−63]

As shown in Figure 1b, the conjugated polymer P, **IDT-TC**, and ICT-IC-Cl exhibit the complementary absorption spectra with each other. The energy levels of these materials (Figure 5) also indicate that combination of these materials is also beneficial for ternary PSCs. The V_{OC} of the **IDT-TC**-based PSC was relatively high compared to that of IDT-IC-Cl, whereas the value of J_{SC} for IDT-IC-Cl was higher than that for **IDT-TC**; we fabricated the ternary PSCs via incorporating **IDT-TC** into the P: IDT-IC-Cl binary active layer. Moreover, the absorption profile of both the acceptors is complementary. The weight concentration of P is held constant, while the weight ratio between the two acceptors is changed from 0.1:1.1 to 0.4:0.8. Additionally, we maintained a total concentration of 14 mg/mL for each ternary blend, the same as for binary blends. We noticed that the best photovoltaic performance was achieved using the ternary active layer P:**IDT-TC**: IDT-IC-Cl (1:0.3:0.9) (Table S3, Supporting Information). The optimized ternary active layer was then subjected to solvent vapor annealing for 40 s as done for binary active layers. Table 3 contains the photovoltaic parameters that correspond to the $J-V$ characteristics under illumination shown in Figure 7a. The PCE for the optimized ternary PSCs reached 16.44%, which is greater than the PCE for the binary PSCs. We also carried out EQE measurements of the ternary PSC in order to learn more about the advancement in the J_{SC} value, as shown in Figure 7b. The P: IDT-IC-Cl binary PSC showed EQE spectra up to 890 nm with a value of around 670 nm, whereas the EQE spectra of the P: **IDT-TC**-based PSC are limited to 780 nm with high values of EQE in the 630−720 nm region. This region is greatly filled up with the addition of **IDT-TC**, which also results in a ternary PSC feature that is broader and more photoresponsive. The EQE spectral difference (ΔEQE) between ternary P: **IDT-TC**: IDT-IC-Cl and binary P: IDT-IC-Cl was also calculated and is shown in Figure S10 (Supporting Information). The ΔEQE values were positive in the spectral range from 300 to 900 nm and highest in the wavelength range where **IDT-TC** had strong absorption, indicating that introduction of **IDT-TC** in the host binary P: ITD-IC-Cl enhances the exciton utilization by the optimized phase of the active ternary layer, thereby leading to the high value of J_{SC}.[64] According to EQE spectra, J_{SC} has an estimated value of 23.75 mA/cm^2, which is in line with the value determined by studying $J-V$ characteristics under illumination. The V_{OC} value for ternary PSC lies in between the PSC based on binary P: IDT-IC-Cl and P: **IDT-TC**, demonstrating that the mixer of these two acceptors forms an alloy and behaves as one acceptor.[65] The value of series resistance (R_s) was

https://doi.org/10.1021/acsomega.2c05141
ACS Omega 2023, 8, 1989−2000

estimated from the slope of $J-V$ curves around the open circuit and found to be 31.43, 38.23, 29.21, and 19.23 Ω for **IDT-TC**, IDT-IC, IDT-Cl, and **IDT-TC**:**IDT-TC**-Cl-based devices, respectively. The lowest value of R_s for the ternary device is in agreement with the highest value of FF for ternary PSCs.[66]

In order to elucidate the influence of the second acceptor on charge transport mechanisms, we measured the hole mobility (μ_h) and electron mobility (μ_e) in the optimized binary and active ternary layers by the space charge limited current model[67] (Figure S11, Supporting Information). P:**IDT-TC** shows concurrently high values of μ_h (5.07×10^{-4} cm^2/Vs) and μ_e (3.97×10^{-4} cm^2/Vs) with a μ_h/μ_e ratio of 1.28 relative to that of P:IDT-IC-Cl ($\mu_h = 4.71 \times 10^{-4}$ cm^2/Vs and μ_e = $3.36 \times 10\text{-}4$ cm^2/Vs with a μ_h/μ_e ratio = 1.40), which may be one reason for a higher value of FF for the P:**IDT-TC**-based PSC as compared to that for P:IDT-IC-Cl. Moreover, compared to binary P:IDT-IC-Cl, the incorporation of **IDT-TC**, that is, optimized ternary one, delivers increased values of both μ_h (5.19×10^{-4} cm^2/Vs) and μe (4.36×10^{-4} cm^2/Vs) with a μ_h/μ_e ratio of 1.19. The fact that both μ_h and μ_e increased for the ternary active layer may be attributed to the increased crystallinity and phase separation nanoscale morphology. This better and balanced charge transfer in the active ternary layer is suggested by the higher values of J_{SC} and FF as well as the lower μ_h/μ_e ratio and greater μ_h and μ_e.[68] The change of photocurrent density (J_{ph}) with effective voltage (V_{eff}) curves was used to explore the production of exciton and their subsequent dissociation into charge generating features (Figure 8). Under the conditions of a short circuit and the

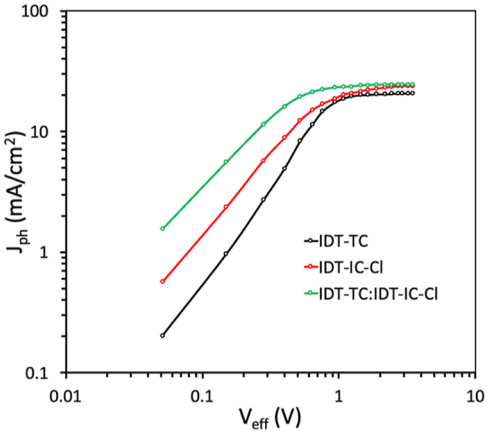

Figure 8. $J_{ph}-V_{eff}$ plots for binary and ternary PSCs.

maximum power point, respectively, the exciton dissociation probability (P_{diss}) and change collection probability (P_{coll}) were estimated from the ratio of J_{ph}/J_{sat}.[69,70] J_{sat} is the value of J_{ph} at high reverse bias, that is, high value of V_{eff}. The P:**IDT-TC** binary PSC attains both higher P_{diss} (0.963) and P_{coll} (0.782) than P:IDT-IC-Cl (P_{diss} = 0.954 and P_{coll} = 0.754). In comparison to its binary counterparts, the ternary P:**IDT-TC**:IDT-IC-Cl-based device displayed higher values of P_{diss} (0.984) and P_{coll} (0.834), demonstrating that the ternary PSC is more effective at both exciton dissociation and charge collection. Additionally, the maximum exciton generation rate (G_{max}) is correlated with J_{sat} by $G_{max} = J_{sat}/qL$ (where q is the elementary charge and L is the thickness of the active layer). J_{sat} for ternary systems is greater than for binary equivalents, suggesting that more excitons are produced in the active ternary layer, which results in a larger value of J_{SC}. G_{max} for the ternary PSC is higher than for binary P:**IDT-TC** and P:IDT-IC-Cl.

The degree of recombination is a key factor in determining the PCE of PSCs, in addition to exciton dissociation and charge collection. Therefore, as shown in Figure 9, we investigated J_{SC} and V_{OC} dependence on incident power intensity. The J_{SC} varies with P_{in} as $J_{SC} \propto (P_{in})^{\alpha}$, where α is the power exponent, which indicates the degree of bimolecular recombination. The bimolecular recombination is almost negligible when α is close to unity.[71] We have estimated the value of α from the J_{SC}-P_{in} plots (Figure 9a). P: IDT-IC-Cl showed a small value of 0.942 than P: **IDT-TC** (0.964), demonstrating a higher bimolecular recombination in the P: IDT-IC-Cl-based binary PSC. However, compared to binary P:IDT-IC-Cl and P:**IDT-TC** devices, the value of α was increased to 0.976 for the optimized ternary device, demonstrating that the introduction of **IDT-TC** into the binary P:IDT-IC-Cl effectively suppresses the bimolecular recombination, which is beneficial for attaining high values of both J_{SC} and FF. The variation of V_{OC} with P_{in} also gives information about another type of recombination, that is, trap-assisted recombination (Figure 9b). The variation of V_{OC} with P_{in} (Figure 9b) can be expressed as $V_{OC} = (nkT/q)\ln P_{in}$, where n is the diode ideality factor, k is the Boltzmann's constant, and T is the absolute temperature. The values of n are estimated to be 1.32, 1.25, and 1.15 for optimized P: IDT-IC-Cl, **IDT-TC**, and P:**IDT-TC**: IDT-IC-Cl, respectively. It is well known that when the value of n is close to 2, trap-assisted recombination predominates in PSCs under open-circuit circumstances. In contrast, bimolecular recombination predominates if the value of n is close to unity.[72] As evidenced by the greatest values of J_{SC} and FF, the lowest value of n for ternary PSCs suggests the least amount of trap-assisted recombination in ternary PSCs.[73]

The charge carrier dynamics are also analyzed by transient photocurrent (TPC) and transient photovoltage (TPV) measurements. We have estimated the charge extraction time (τ_{ext}) by fitting the TPC decays under short-circuit conditions[74] (Figure 10a). The τ_{ext} values for P: IDT-IC-Cl and the ternary P:**IDT-TC**: IDT-IC-Cl are fitted to be 3.67 and 2.39 μs, respectively. Small τ_{ext} for the ternary device indicates promoted efficiency of charge sweep-out and demonstrates the faster charge extraction than the binary counterpart. Furthermore, TPC under open-circuit conditions is performed to get information about the charge carrier lifetime and reflect the recombination time of the photocharge carrier (τ_{rec}).[75] The τ_{rec} values estimated from the TPC plots (Figure 10b) for the ternary device are about 8.34 μs, which is higher than that for the binary counterpart (6.45 μs), demonstrating the effective suppression of charge recombination in the ternary PSC. Therefore, these results again validate the superior charge extraction and suppressed charge recombination loss in the ternary PSC.

We have compared the absorption spectra of IDT-IC-Cl and steady-state photoluminescence (PL) spectra of **IDT-TC** to investigate the intermolecular dynamic process between these two acceptors. As presented in Figure 11a, most of the PL spectra of **IDT-TC** overlapped with the PL absorption spectra of IDT-IC-Cl, demonstrating effective energy transfer from **IDT-TC** to IDT-IC-Cl in line with Forster theory.[76,77] In order to verify this energy transfer process, we have recorded the PL spectra of IDT-IC-Cl, **IDT-TC**, and their blend, which are

https://doi.org/10.1021/acsomega.2c05141
ACS Omega 2023, 8, 1989−2000

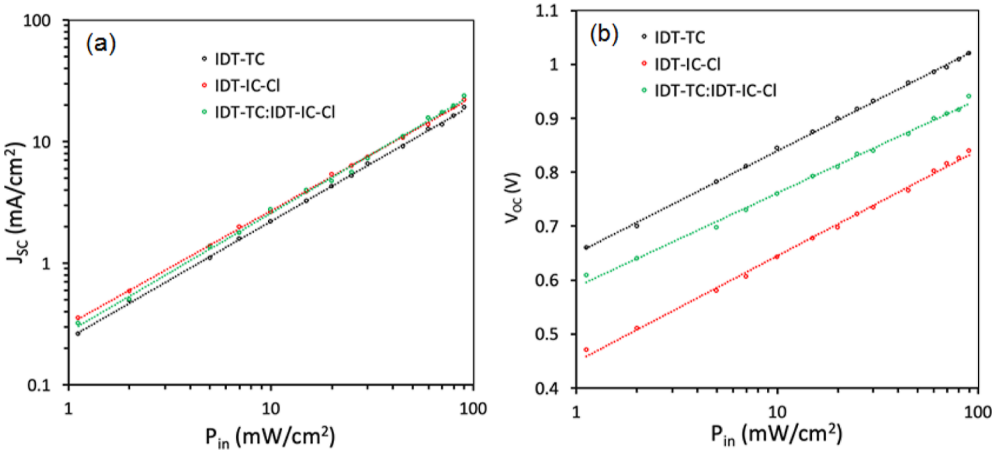

Figure 9. Variations of (a) J_{SC} and (b) V_{OC} with P_{in} for binary and ternary devices.

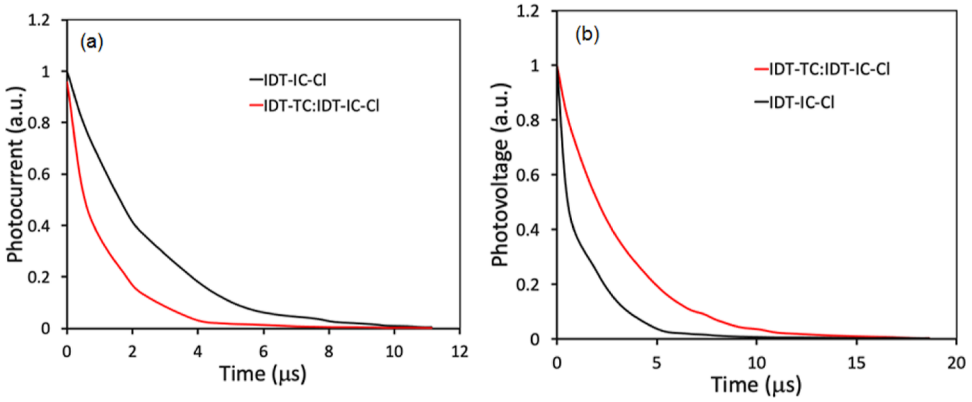

Figure 10. (a) TPC and (b) TPV curves for binary and ternary devices.

presented in Figure 11b. The PL emission of **IDT-TC** was efficiently quenched in **IDT-TC**:IDT-IC-Cl, whereas the intensity of the PL emission peak located at 888 nm is significantly increased, revealing the efficient energy transfer between **IDT-TC** and IDT-IC-Cl[78] as presented in Figure 11c.

We constructed the devices using the pristine acceptors, and their optimum blend and $J-V$ characteristics were examined to learn more about the potential for charge (electrons and holes) transfer between two acceptors. We found that the J_{SC} values of the device based on the blend of acceptors lie between the pure acceptor devices, indicating that charge transfer between two acceptors does not occur. The possible energy transfer and charge transfer that occurred in the ternary device are presented in Figure 11c. The transfer of electrons from polymer donor P to **IDT-TC** or IDT-IC-Cl and holes from either **IDT-TC** or IDT-IC-Cl occur. Therefore, more D/A interfaces (P/**IDT-TC** and P/IDT-IC-Cl) are created in the active ternary layer, whereas only P/IDT-IC-Cl interfaces are present in the active binary layer. As the number of interfaces depends upon the morphology of the blended film and D/A ratio, the more creation of D/A interfaces owing to the nanoscale morphology of the ternary active layer is beneficial for enhanced exciton dissociation. In the ternary active layer-based PSC, the effective utilization of exciton occurs via energy transfer from **IDT-TC** to IDT-IC-Cl, thereby enhancing the exciton generation rate and leading to a high value of J_{SC}.

3.7. TEM and XRD Results. An essential factor that affects the photovoltaic performance of PSCs, especially the J_{SC} and FF, is the molecular crystallinity and morphology of the active layer. Therefore, we have examined the molecular crystallinity of the binary (P:IDT-IC-Cl) and ternary (P:**IDT-TC**:IDT-IC-Cl) films via recording the XRD patterns as displayed in Figure 12. Both binary and ternary films showed two diffraction peaks at $2\theta = 5.63/6.09°$ (corresponds to lamellar stacking) and $2\theta = 24.09/24.78°$ (corresponds to $\pi-\pi$ stacking), respectively. The d-spacing and $\pi-\pi$ stacking distances for binary and ternary films are 1.59/0.361 and 1.47/0.351 nm, respectively. The crystal coherence distances (CCLs) corresponding to lamellar stacking/$\pi-\pi$ stacking for binary and ternary films are 5.22/6.47 and 3.48/3.53 nm, respectively. It is advantageous for effective charge transport, which lowers charge recombination and supports high values of J_{SC} and FF, to have a greater value of CCL (owing to the higher crystallinity of **IDT-TC**) and a smaller value of $\pi-\pi$ stacking distance for the ternary film.

Figure 13 depicts the results of a morphological analysis performed using transmission electron microscopy (TEM) on the active layers. The active ternary films exhibit enhanced phase separation because the domain size in ternary films is larger than that in their binary counterparts. This improved phase separation can help facilitate exciton dissociation and suppress charge recombination via balanced charge transport, resulting in a greater value of FF.

4. CONCLUSIONS

In this work, we developed a novel medium bandgap non-fullerene SMA called **IDT-TC**, which is built on an IDT donor

https://doi.org/10.1021/acsomega.2c05141
ACS Omega 2023, 8, 1989−2000

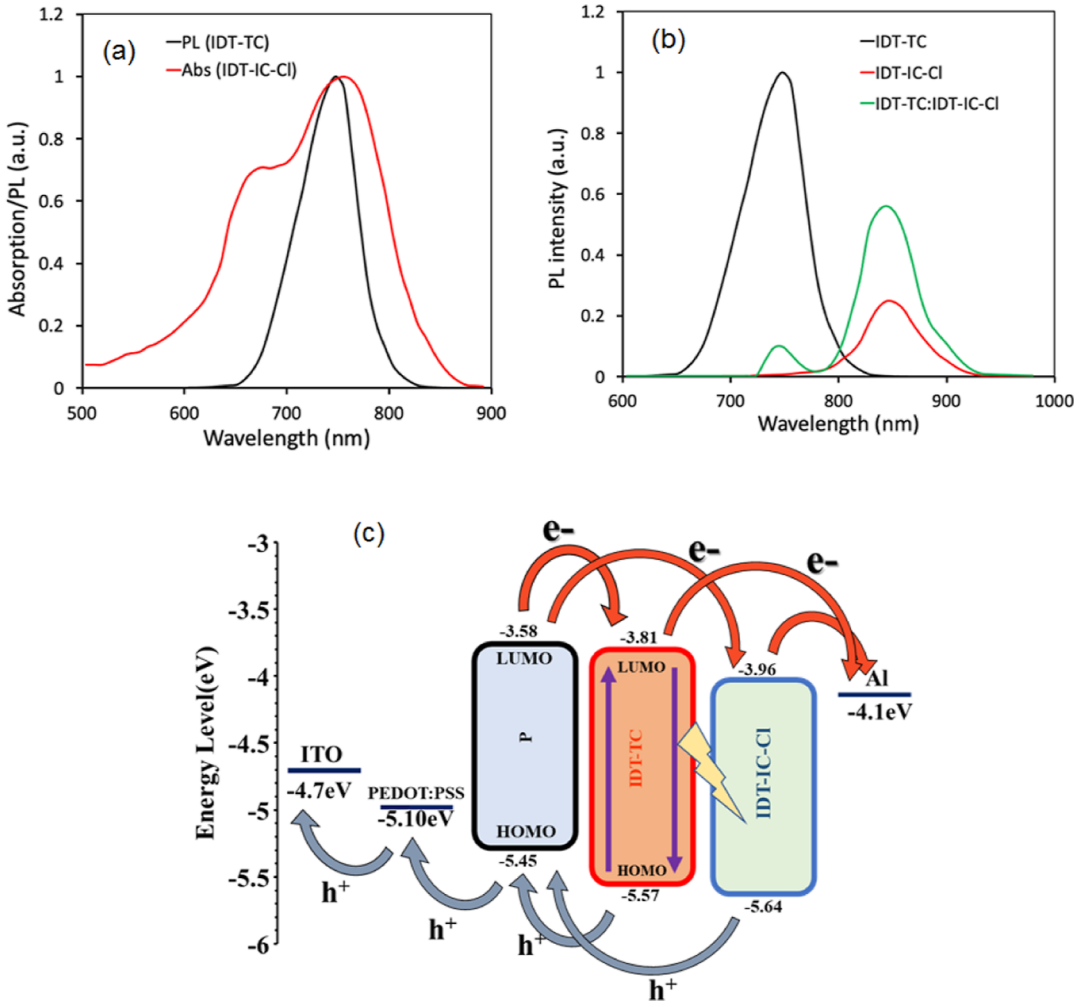

Figure 11. (a) Thin-film PL spectra of **IDT-TC** and absorption spectra of IDT-IC-Cl, (b) thin-film PL spectra of pristine **IDT-TC**, IDT-IC-Cl, and optimized **IDT-TC**:IDT-IC-Cl, and (c) working mechanism of the ternary PSC.

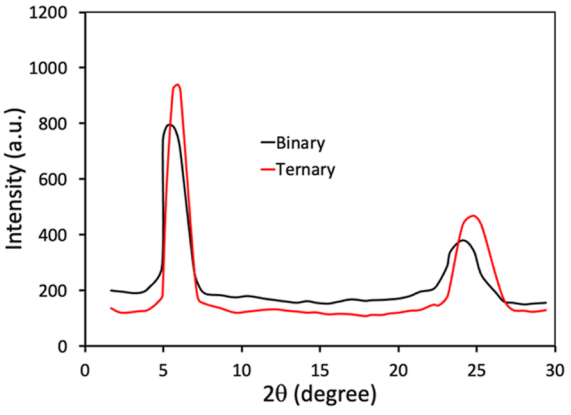

Figure 12. XRD patterns of binary (P:IDT-IC-Cl) and ternary (P:**IDT-TC**:IDT-IC-Cl) films.

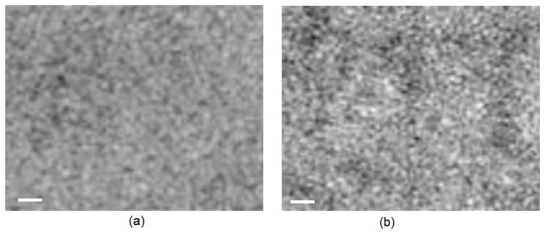

Figure 13. TEM images of optimized (a) P:IDT-IC-Cl and (b) P:**IDT-TC**:IDT-IC-Cl films. The scale bar is 100 nm.

core and TC acceptor terminals. We compared its optical and electrochemical characteristics with those of IDT-IC. **IDT-TC** showed upshifted LUMO energy levels compared to IDT-IC. The PSCs based on P: **IDT-TC** demonstrated a PCE of 14.26% using a wide bandgap D−A conjugated polymer P, which is higher than that of the IDT-IC counterpart (11.56%). The greater values of FF and V_{OC} for the **IDT-TC**-based device are responsible for the PCE, despite the fact that the J_{SC} for the PSC based on IDT-IC is higher than that for **IDT-TC**. We have also fabricated the PSCs using a narrow bandgap NFA IDT-IC-Cl, and the P: IDT-IC-Cl-based device showed a PCE of 13.34%. We have included **IDT-TC** in P: IDT-IC-Cl as a guest acceptor to construct the ternary PSCs, taking advantage of greater values of J_{SC} for the IDT-IC-Cl counterpart and higher values of V_{OC} and FF for the binary BHJ PSCs based on **IDT-TC**. Following optimization, the ternary PSCs displayed a fantastic PCE of 16.44% (J_{SC} = 23.98 mA/cm^2, V_{OC} = 0.98 V, and FF = 0.714). Faster charge extraction in the ternary PSCs, more balanced charge transport, less charge recombination, and the usage of excitons via energy transfer from **IDT-TC** to IDT-IC-Cl are all factors that contribute to PCE's higher value. Additionally, the active

https://doi.org/10.1021/acsomega.2c05141
ACS Omega 2023, 8, 1989−2000

ternary layer's compact stacking distance and proper phase separation also contribute to the values of FF and J_{SC} in the ternary PSCs.

■ ASSOCIATED CONTENT

Supporting Information

The Supporting Information is available free of charge at https://pubs.acs.org/doi/10.1021/acsomega.2c05141.

Instrumentation, synthesis of intermediate compounds, ^{1}H NMR spectra and ^{13}C NMR spectra of **IDT-TC**, TGA spectra, molecular geometries of **IDT-TC**, device fabrication method, dark $J-V$ characteristics of the devices to estimate the charge carrier mobilities, XRD patterns of pristine films, PL spectra, and photovoltaic parameters of optimization of the performance of PSCs (PDF)

■ AUTHOR INFORMATION

Corresponding Authors

Mukhamed L. Keshtov − *A.N. Nesmeyanov Institute of Organoelement Compounds of the Russian Academy of Sciences, Moscow 119991, Russian Federation*; Email: keshtov@ineos.ac.ru

Ganesh D. Sharma − *Department of Physics, The LNM Institute of Information Technology, Jaipur 302031 Rajasthan, India; Department of Electronics and Communication Engineering, The LNM Institute of Information Technology, Jaipur 302031 Rajasthan, India;* orcid.org/0000-0002-1717-0116; Email: gdsharma273@gmail.com

Authors

Alexei R. Khokhlov − *A.N. Nesmeyanov Institute of Organoelement Compounds of the Russian Academy of Sciences, Moscow 119991, Russian Federation*

Dimitriy Y. Shikin − *A.N. Nesmeyanov Institute of Organoelement Compounds of the Russian Academy of Sciences, Moscow 119991, Russian Federation*

Vladimir Alekseev − *Inorganic and Analytical Chemistry Department, Tver State University, Tver 170002, Russian Federation*

Giriraj Chayal − *Department of Physics, Jai Narain Vyas University, Jodhpur 342005 Rajasthan, India*

Hemraj Dahiya − *Department of Physics, The LNM Institute of Information Technology, Jaipur 302031 Rajasthan, India;* orcid.org/0000-0002-1427-2758

Manish Kumar Singh − *Department of Physics, The LNM Institute of Information Technology, Jaipur 302031 Rajasthan, India*

Fang Chung Chen − *Department of Photonics and Center for Emergent Functional Matter Science, National Yang Ming Chiao Tung University, Hsinchu 30010, Taiwan;* orcid.org/0000-0002-4131-3893

Complete contact information is available at: https://pubs.acs.org/10.1021/acsomega.2c05141

Author Contributions

All the authors have contributed equally and have given approval to the final version of the manuscript.

Notes

The authors declare no competing financial interest.

■ ACKNOWLEDGMENTS

This work was supported by the Ministry of Science and Higher Education of the Russian Federation (contract/agreement no. 075-00697-22-00) and was performed employing the equipment of the Center for molecular composition studies of INEOS RAS. G.D.S. is thankful to the Department of Science and Technology for providing the financial support through BRICS and Indo-Taiwan project.

■ REFERENCES

(1) Yu, G.; Gao, J.; Hummelen, J. C.; Wudl, F.; Heeger, A. J. Polymer Photovoltaic Cells: Enhanced Efficiencies via a Network of Internal Donor-Acceptor Heterojunction. *Science* **1995**, *270*, 1789−1791.

(2) Lee, S.; Jeong, D.; Kim, C.; Lee, C.; Kang, H.; Woo, H. Y.; Kim, B. J. Eco-friendly polymer solar cells: Advance in Green Solvent Processing and Material Design. *ACS Nano* **2020**, *14*, 14493−14527.

(3) Chen, H.; Zhang, R.; Chen, X.; Zeng, G.; Kobera, L.; Abbrent, S.; Zhang, B.; Chen, W.; Xu, G.; Oh, J.; Kang, S.-H.; Chen, S.; Yang, C.; Brus, J.; Hou, J.; Gao, F.; Li, Y.; Li, Y. A Guest-Assisted Molecular Organization Approach for >17 % Efficiency Organic Solar Cells Using Environmentally Friendly Solvents. *Nat. Energy* **2021**, *6*, 1045−1053.

(4) Lu, L.; Zheng, T.; Wu, Q.; Schneider, A. M.; Zhao, D.; Yu, L. Recent Advances in Bulk Heterojunction Polymer Solar Cells. *Chem. Rev.* **2015**, *115*, 12666−12731.

(5) Duan, L.; Uddin, A. Progress in Stability of Organic Solar Cells. *Adv. Sci.* **2020**, *7*, 1903259.

(6) Chen, L. X. Organic solar cells: Recent Progress and Challenges. *ACS Energy Lett.* **2019**, *4*, 2537−2539.

(7) Hong, L.; Yao, H.; Cui, Y.; Ge, Z.; Hou, J. Recent Advances in Highly Efficiency Organic Solar Cells Fabricated by Eco-compatible Solvents at Relatively Large Area Scale. *APL Mater.* **2020**, *8*, 120901.

(8) Yang, F.; Huang, Y.; Li, Y.; Li, Y. Large-Area Flexible Organic Solar Cells. *npj Flexible Electron.* **2021**, *5*, 30.

(9) Yuan, J.; Zhang, Y.; Zhou, L.; Zhang, G.; Yip, H.-L.; Lau, T.-K.; Lu, X.; Zhu, C.; Peng, H.; Johnson, P. A.; Leclerc, M.; Cao, Y.; Ulanski, J.; Li, Y.; Zou, Y. Single Junction Organic Solar Cell with Over 15 % Efficiency Using Fused Ring Acceptor with Electron-Deficient Core. *Joule* **2019**, *3*, 1140−1151.

(10) Jiang, K.; Wei, Q.; Lai, J. Y. L.; Peng, Z.; Kim, H. K.; Yuan, J.; Ye, L.; Ade, H.; Zou, Y.; Yan, H. Alkyl Chain Tunning of Small Molecule Acceptors for Efficient Organic Solar Cells. *Joule* **2019**, *3*, 3020−3033.

(11) Xu, X.; Qi, Y.; Luo, X.; Xia, X.; Lu, X.; Yuan, J.; Zhou, Y.; Zou, Y. Alkyl Side-Chain Engineering Enables High Performance As Cast Organic Solar Cells of Over 17 % Efficiency. *Fundam. Res.* **2022**, DOI: 10.1016/j.fmre.2022.01.025.

(12) Bi, P.; Zhang, S.; Chen, Z.; Xu, Y.; Cui, Y.; Zhang, T.; Ren, J.; Qin, J.; Hong, L.; Hao, X.; Hou, J. Reduced Non-radiative Charge Recombination Enables Organic Photovoltaic Cell Approaching 19 % Efficiency. *Joule* **2021**, *5*, 2408−2419.

(13) Chong, K.; Xu, X.; Meng, H.; Xue, J.; Yu, L.; Ma, W.; Peng, Q. Realizing 19.05 % Efficiency Polymer Solar Cells by Progressively Improving Charge Extraction and Suppressing Charge Recombination. *Adv. Mater.* **2022**, *34*, No. e2109516.

(14) Bao, S.; Yang, H.; Fan, H.; Zhang, J.; Wei, Z.; Cui, Y.; Li, Y. Volatilizable Solid additive Assisted Treatment Enables Organic Solar Cells with Efficiency Over 18.8 % and Fill Factor Exceeding 80. *Adv. Mater.* **2021**, *33*, No. e2105301.

(15) Zhang, M.; Zhu, L.; Zhou, G.; Hao, T.; Qiu, C.; Zhao, Z.; Hu, Q.; Larson, B. W.; Zhu, H.; Ma, Z.; Tang, Z.; Feng, W.; Zhang, Y.; Russell, T. P.; Liu, F. Single Layered Organic Photovoltaics With Double Cascading Charge Transport Pathways:18 % Efficiencies. *Nat. Commun.* **2021**, *12*, 309.

(16) Zhang, X.; Li, C.; Xu, J.; Wang, R.; Song, J.; Zhang, H.; Li, Y.; Jing, G.; Li, J.; Wu, X.; Zhou, Y.; Li, X.; Zhang, J.; Li, C.; Zhang, H.; Zhang, Y.; Zhou, Y.; Sun, Y.; Zhang, Y. High Fill Factor Solar Cells

with Increased Dielectric Constant and Molecular Packing Density. *Joule* **2022**, *6*, 444−457.
(17) Li, X.; Luo, S.; Sun, H.; Sung, H. H. Y.; Yu, H.; Liu, T.; Xiao, Y.; Bai, F.; Pan, M.; Lu, X.; Williams, I. D.; Guo, X.; Li, Y.; Yan, H. Medium Bandgap Nonfulluerene Acceptors Based on Benzothiophene Donor Moiety Enabling High Performance Indoor Organic Photovoltaics. *Energy Environ. Sci.* **2021**, *14*, 4555−4563.
(18) Ahn, J.; Oh, S.; Lee, H.; Lee, S.; Song, C. E.; Lee, H. K.; Lee, S. K.; So, W. W.; Moon, S. J.; Lim, E.; Shin, W. S.; Lee, J. C. Simple and Versatile Nonfullerene Acceptor Based Benzothiadiazole and Rhodanine for Organic Solar Cells. *ACS Appl. Mater. Interfaces* **2019**, *11*, 30098−30107.
(19) Wang, Y.; Chang, M.; Ke, X.; Wan, X.; Yang, G. A New Medium Bandgap Fused-[1]benzothieno[3,2-b]]1]benzo-thiophene (BTBT) Nonfullerene Acceptor for Organic Solar Cells with High Open Circuit Voltage. *Polymer* **2019**, *185*, 121976.
(20) Cheng, P.; Li, G.; Zhan, X.; Yang, Y. Next Generation Organic Photovoltaics Based on Non-fullerene Acceptors. *Nat. Photonics* **2018**, *12*, 131−142.
(21) Li, S.; Liu, W.; Li, C. Z.; Shi, M.; Chen, H. Efficient Organic Solar Cells with Non-fullerene Acceptors. *Small* **2017**, *13*, 1701120.
(22) Hou, J.; Inganäs, O.; Friend, R. H.; Gao, F. Orgnaic Solar Cells Based on Non-fullerene Ccceptors. *Nat. Mater.* **2018**, *17*, 119−128.
(23) He, B.; Yang, B.; Kolaczkowski, M. A.; Anderson, C. A.; Klivansky, L. M.; Chen, T. L.; Brady, M. A.; Liu, Y. Molecular Engineering for Large Open Circuit Voltage and Low Energy Loss in Around 10 % Non-fullerene Organic Photovoltaics. *ACS Energy Lett.* **2018**, *3*, 1028−1035.
(24) Zhang, G.; Zhao, J.; Chow, P. C. Y.; Jiang, K.; Zhang, J.; Zhu, Z.; Zhang, J.; Huang, F.; Yan, H. Nonfullerene Acceptor Molecules for Bulk Heterojunction Organic Solar Cells. *Chem. Rev.* **2018**, *118*, 3447−3507.
(25) Fan, Q.; Xu, Z.; Guo, X.; Meng, X.; Li, W.; Su, W.; Ou, X.; Ma, W.; Zhang, M.; Li, Y. High-Performance Nonfullerene Polymer Solar Cells with Open-Circuit Voltage Over 1.0 V and Energy Loss as Low as 0.54 eV. *Nano Energy* **2017**, *40*, 20−26.
(26) Cui, Y.; Yao, H.; Gao, B.; Qin, Y.; Zhang, S.; Yang, B.; He, C.; Xu, B.; Hou, J. Fine Tuned Photoactive and Interconnection Layers for Achieving over 13 % Efficiency in a Fullerene Free Tandem Organic Solar Cell. *J. Am. Chem. Soc.* **2017**, *139*, 7302−7309.
(27) Liu, G.; Jia, J.; Zhang, K.; Jia, X.; Yin, Q.; Zhong, W.; Li, L.; Huang, F.; Cao, Y. 15 % Efficiency Tandem Organic Solar Cells Based on a Novel Highly Efficient Wide Bandgap Nonfullerene Acceptor with Low Energy Loss. *Adv. Energy Mater.* **2019**, *9*, 1803657.
(28) Meng, L.; Yi, Y.-Q.-Q.; Wan, X.; Zhang, Y.; Ke, X.; Kan, B.; Wang, Y.; Xia, R.; Yip, H.-L.; Li, C.; Chen, Y. A Tandem Organic Solar Cell with PCE of 14.25 % Employing Subcells with the Same Polymer Donor and Two Absorption Complementary Acceptors. *Adv. Mater.* **2019**, *31*, 1804723.
(29) Cheng, P.; Liu, Y.; Chang, S. Y.; Li, T.; Sun, P.; Wang, R.; Cheng, H. W.; Huang, T.; Meng, L.; Nuryyeva, S.; Zhu, C.; Wei, K. H.; Sun, B.; Zhan, X.; Yang, Y. Efficient Tandem Organic Photovoltaics with Tunable Rear Sub-cells. *Joule* **2019**, *3*, 432−442.
(30) Zhang, Y.; Kan, B.; Sun, Y.; Wang, Y.; Xia, R.; Ke, X.; Yi, Y. Q. Q.; Li, C.; Yip, H. L.; Wan, X.; Cao, Y.; Chen, Y. Nonfullerene Tandem Organic Solar Cells with High Performance of 14 .11. *Adv. Mater.* **2018**, *30*, 1707508.
(31) Meng, L.; Zhang, Y.; Wan, X.; Li, C.; Zhang, X.; Wang, Y.; Ke, X.; Xiao, Z.; Ding, L.; Xia, R.; Yip, H. L.; Cao, Y.; Chen, Y. Organic and Solution Processed Tandem Solar Cells with 17 .3 % Efficiency. *Science* **2018**, *361*, 1094−1098.
(32) Liu, Q.; Jin, K.; Li, W.; Xiao, Z.; Cheng, M.; Yuan, Y.; Shi, S.; Jin, Z.; Hao, F.; Yang, S.; Ding, L. An Efficient Medium Bandgap Nonfullerene Acceptor for Organic Solar Cells. *J. Mater. Chem. A* **2020**, *8*, 8857−8861.
(33) Liu, G.; Xia, R.; Huang, Q.; Zhang, K.; Hu, Z.; Jia, T.; Liu, X.; Yip, H. L.; Huang, F. Tandem Organic Solar Cells with 18.7 % Efficiency Enabled by Suppressing the Charge Recombination in Front Sub-cell. *Adv. Funct. Mater.* **2021**, *31*, 2103283.
(34) Di Carlo Rasi, D.; Janssen, R. A. J. Advances in Solution-Processed Multijunction Organic Solar Cells. *Adv. Mater.* **2019**, *31*, 18064999.
(35) Zhang, M.; Wang, J.; Ma, X.; Gao, J.; Xu, C.; Hu, Z.; Niu, L.; Zhang, F. Review on Smart Strategies for Achieving Highly Efficient Ternary Polymer Solar Cells. *APL Mater.* **2020**, *8*, 090703.
(36) Doumon, N. Y.; Yang, L.; Rosei, F. Ternary Organic Solar Cells: A Review of the Role of the Third Element. *Nano Energy* **2022**, *94*, 106915.
(37) Zhang, X.; Wang, Q.; Shen, W.; Han, C.; Shao, Y.; Belfiore, L. A.; Tang, J. Recent advances and prospects of D1:D2:A non-fullerene ternary polymer solar cells. *J. Mater. Chem. C* **2021**, *9*, 41−66.
(38) Zhao, C.; Wang, J.; Zhao, X.; Du, Z.; Yang, R.; Tang, J. Recent advances, Challenges and Prospects in Ternary Organic Solar Cells. *Nanoscale* **2021**, *13*, 2181−2208.
(39) Wang, T.; Wang, X.; Yang, R.; Li, C. Recent Advances in Ternary Organic Solar Cells Based on Förster Resonance Energy Transfer. *Solar RRL* **2021**, *5*, 2100496.
(40) Gasparini, N.; Salleo, N. A.; McCulloch, I.; Baran, D. The role of the third component in ternary organic solar cells. *Nat. Rev. Mater.* **2019**, *4*, 229−242.
(41) Cheng, H. W.; Juan, C. Y.; Mohapatra, A.; Chen, C. H.; Lin, Y. C.; Chang, B.; Cheng, P.; Wang, H. C.; Chu, C. W.; Yang, Y.; Wei, K. H. High-Performance Organic Photovoltaics Incorporating an Active Layer with a Few Nanometer-Thick Third-Component Layer on a Binary Blend Layer. *Nano Lett.* **2021**, *21*, 2207−2215.
(42) Sharma, G. D.; Agrawal, A.; Pradhan, R.; Keshtov, M. L.; Singhal, R.; Liu, W.; Zhu, X.; Mishra, A. Fullerene-Free All-Small-Molecule Ternary Organic Solar Cells with Two Compatible Fullerene-Free Acceptors and a Coumarin Donor Enabling a Power Conversion Efficiency of 14.5. *ACS Appl. Energy Mater.* **2021**, *4*, 11537−11544.
(43) Privado, M.; Dahiya, H.; de la Cruz, P.; Keshtov, M. L.; Langa, F.; Sharma, G. D. A Ternary Organic Solar Cell with 15.6 % Efficiency Containing a New DPP-Based Acceptor. *J. Mater. Chem. C* **2021**, *9*, 16272−16281.
(44) Suman, S. P.; Singh, S. P. Impact of End Groups on the Performance of Non-fullerene Acceptors for Organic Solar Cell Applications. *J. Mater. Chem. A* **2019**, *7*, 22701−22729.
(45) Liu, S.; Zhao, B.; Cong, Z.; Cheng, Q.; Wang, W.; Pan, H.; Liu, J.; Wu, H.; Gao, C. Influence of the Terminal Groups on the of Small Molecule Acceptors- Based Polymer Solar Cell. *Dyes Pigments* **2020**, *178*, 108388.
(46) Qiu, N.; Zhang, H.; Wan, X.; Li, C.; Ke, X.; Feng, H.; Kan, B.; Zhang, H.; Zhang, Q.; Lu, Y.; Chen, Y. A New Nonfullerene Electron Acceptor with a Ladder Type Backbone for High-Performance Organic Solar Cells. *Adv. Mater.* **2017**, *29*, 1604964.
(47) Zhang, Q.; Adil, M. A.; Wang, Z.; Zhao, G.; Wang, T.; Jiang, R.; Zhang, Q.; Wang, Q. Influence of the terminal group on optoelectronic properties of fused-ring nonfullerene acceptors with ethylhexyl side chain. *Dyes Pigm.* **2021**, *194*, 109635.
(48) Zhang, Z.; Feng, L.; Xu, S.; Yuan, J.; Zhang, Z. G.; Peng, H.; Li, Y.; Zou, Y. Achieving Over 10 % Efficiency in a New Ccceptor ITTC and Its Blends with Hexafluoriquinoxaline Based Polymers. *J. Mater. Chem. A* **2017**, *5*, 11286−11293.
(49) Liao, L.; Zheng, P.; Cai, Z.; Shen, S.; Xu, G.; Zhao, H.; Xu, Y. Construction of Simple and Low Cost Acceptors for Efficient Non-fullerene Orgnaic Solar Cells. *Organ. Electron.* **2021**, *89*, 106026.
(50) Zhang, Y.; Cai, F.; Yuan, J.; Wei, Q.; Zhou, L.; Qiu, B.; Hu, Y.; Li, Y.; Peng, H.; Zou, Y. A New Non-fullerene Acceptor Based on the Combination of a Heptacyclic Benzothiazole Unit and a Thiophene Fused End Group Cchieving Over 13 % Efficiency. *Phys. Chem. Chem. Phys.* **2019**, *21*, 26557.
(51) Xie, D.; Liu, T.; Gao, W.; Zhong, C.; Huo, L.; Luo, Z.; Wu, K.; Xiong, W.; Liu, F.; Sun, Y.; Yang, C. A Novel Thiophene Fused Ending Group Enabling an Excellent Small Molecule Acceptor for High-Performance Fullerene Free Polymer Solar Cells With 11.8 % Efficiency. *Solar RRL* **2017**, *1*, 1700044.

https://doi.org/10.1021/acsomega.2c05141
ACS Omega 2023, 8, 1989−2000

(52) Wu, H.; Bian, Q.; Zhao, B.; Zhao, L.; Wang, W.; Wang, Z.; Cong, J.; Liu, W.; Ma, C.; Gao, C. Effects of the Isomerized Thiophene Fused Ending Groups on the Performance of Twisted Non-fullerene Acceptor-Based Polymer Solar Cells. *ACS Appl. Mater. Interfaces* **2020**, *12*, 23904−23913.
(53) Keshtov, M. L.; Kuklin, S. A.; Dou, C.; Koukaras, E. N.; Singhal, R.; Malhotra, P.; Sharma, G. D. Enhancement of Photovoltaic Efficiency Through Fine Adjustment of Indacene-based Non-fullerene Ccceptor by Minimal Chlorination for Polymer Solar Cells. *Nano Select* **2020**, *1*, 320−333.
(54) Keshtov, M. L.; Kuklin, S. A.; Khokhlov, A. R.; Xie, Z.; Alekseev, V. G.; Dahiya, H.; Singhal, R.; Sharma, G. D. New Medium Bandgap Donor D-A_1-D-A_2 Type Copolymers Based on Anthra[1,2-b: 4,3-b":6,7-c"'] Trithiophene-8,12-dione Groups for High-Efficient Non-Fullerene Polymer Solar Cells. *Macro. Rap. Commun.* **2022**, *43*, 2100839.
(55) Hou, J.; Huo, L.; He, C.; Yang, C.; Li, Y. Synthesis and Absorption Spectra of Poly(3-(phenylenevinyl)thiophene)s with Conjugated Side Chains. *Macromolecules* **2006**, *39*, 594−603.
(56) Yao, H.; Ye, L.; Hou, J.; Jang, B.; Han, G.; Cui, Y.; Su, G. M.; Wang, C.; Gao, B.; Yu, R.; Zhang, H.; Yi, T.; Woo, H. Y.; Ade, H.; Hou, J. Achieving Highly Efficient Nonfullerene Organic Solar Cells with Improved Intermolecular Interaction and Open Circuit Voltage. *Adv. Mater.* **2017**, *29*, 1700254.
(57) Huang, J.; Tang, H.; Yan, C.; Li, G. 1,1-dicyanomethylene-3-indanone End Group Engineering for Fused Electron Acceptor Based High-Performance Organic Photovoltaics. *Cell Rep. Phys. Sci.* **2021**, *2*, 100292.
(58) Chen, S.; Wang, Y.; Zhang, L.; Zhao, J.; Chen, Y.; Zhu, D.; Yao, H.; Zhang, G.; Ma, W.; Friend, R. H.; Chow, P. C. Y.; Gao, F.; Yan, H. Efficient Nonfullerene Organic Solar Cells with Small Driving Force for Both Hole and Electron Transfer. *Adv. Mater.* **2018**, *30*, 1804215.
(59) Li, S.; Zhan, L.; Sun, C.; Zhu, H.; Zhou, G.; Yang, W.; Shi, M.; Li, C. Z.; Hou, J.; Li, Y.; Chen, H. Highly Efficient Fullerene Free Organic Solar Cells Operated at Near Zero Highest Occupied Molecular Orbitals. *J. Am. Chem. Soc.* **2019**, *141*, 3073−3082.
(60) Doumon, N. Y.; Yang, L.; Rosei, F. Ternary Organic Solar Cells: A Review of the Role of the Third Element. *Nano Energy* **2022**, *94*, 106915.
(61) Zhang, S.; Ma, X.; Xu, C.; Xu, W.; Xu, W.; Jeong, S. Y.; Woo, H. Y.; Zhou, Z.; Zhang, X.; Zhang, F.; Zhang, F. Boosted Efficiency Over 18.1 % of Polymer Solar cells by Employing Large Extinction Coefficients Material as the Third Component. *Macro. Rap. Commun.* **2022**, *43*, 2200345.
(62) Ma, X.; Zeng, A.; Gao, J.; Hu, Z.; Xu, C.; Son, J. H.; Jeong, S. Y.; Zhang, C.; Li, M.; Wang, K.; Yan, H.; Ma, Z.; Wang, Y.; Woo, H. Y.; Zhang, F. Approaching 18 % Efficiency of Ternary Organic Photovoltaics with Wide Bandgap Polymer Donor and Well Compatible Y6:Y6-10 as Acceptor. *Nat. Sci. Rev.* **2021**, *8*, nwaa305.
(63) An, Q.; Wang, J.; Gao, W.; Ma, X.; Hu, Z.; Gao, J.; Xu, C.; Hao, M.; Zhang, X.; Yang, C.; Zhang, F. Alloy-Like Ternayr Polymer Solar Cells with Over 17.2 % Efficiency. *Sci. Bull.* **2020**, *65*, 538−545.
(64) Sun, C.; Qin, S.; Wang, R.; Chen, S.; Pan, F.; Qiu, B.; Shang, Z.; Meng, L.; Zhang, C.; Xiao, M.; Yang, C.; Li, Y. High-Efficiency Polymer Solar Cells with Efficient Hole Transfer at Zero Highest Occupied Molecular Orbital Offset Between Methylated Polymer Donor and Brominated Acceptor. *J. Am. Chem. Soc.* **2020**, *142*, 1465−1474.
(65) Jiang, H.; Han, C.; Li, Y.; Bi, F.; Zheng, N.; Han, J.; Shen, W.; Wen, S.; Yang, C.; Yang, R.; Bao, X. Rational Mutual Interactions in Ternary Systems Enable High-Performance Organic Solar Cells. *Adv. Funct. Mater.* **2020**, *31*, 2007088.
(66) Xu, W.; Li, X.; Jeong, S. Y.; Son, J. H.; Zhou, Z.; Jiang, Q.; Woo, H. Y.; Wu, Q.; Zhu, X.; Ma, X.; Zhang, F. Achieving 17.5 % Efficiency for Polymer Solar Cells via Donor and Acceptor Layerd Optimization. *J. Mater. Chem. C* **2022**, *10*, 5489−5496.
(67) Khlyabich, P. P.; Sezen-Edmonds, M.; Howard, J. B.; Thompson, B. C.; Loo, Y. L. Formaion of Organic Alloys in Ternary-Blend Solar Cells with Two Ccceptors Having Energy Level Offsets Exceeding 0.4 eV. *ACS Energy Lett.* **2017**, *2*, 2149−2156.
(68) Röhr, J. A.; Moia, D.; Haque, S. A.; Kirchartz, T.; Nelson, J. Exploring the Validity and Limitations of the Mott-Gurney Law for Charge Carrier Mobility Determination of Semiconducting Thin Films. *J. Phys. Condens. Matter.* **2018**, *30*, 105901.
(69) Song, X.; Gasparini, N.; Nahid, M. M.; Chen, H.; Macphee, S. M.; Zhang, W.; Norman, V.; Zhu, C.; Bryant, D.; Ade, H.; McCulloch, I.; Baran, D. A Highly Crystalline Fused Ring n-type Small Molecule for Nonfullerene Acceptor Based Organic Solar Cells and Field-Effect Transistors. *Adv. Funct. Mater.* **2018**, *28*, 1802895.
(70) Shrotriya, V.; Yao, Y.; Li, G.; Yang, Y. Effect of Self-Organization in Polymer/Fullerene Bulk Heterojunctions on Solar Cell Performance. *Appl. Phys. Lett.* **2006**, *89*, 063505.
(71) Blom, P. W. M.; Mihailetchi, V. D.; Koster, L. J. A.; Markov, D. E. Device Physics of Polymer: Fullerene Bulk Heterojunction Solar Cells. *Adv. Mater.* **2007**, *19*, 1551−1566.
(72) Chen, Y.; Liu, T.; Hu, H.; Ma, T.; Lai, J. Y. L.; Zhang, J.; Ade, H.; Yan, H. Modulation of End Groups for Low Bandgap Nonfullerene Acceptors Enabling High Performance Organic Solar Cells. *Adv. Energy Mater.* **2018**, *8*, 1801203.
(73) Ma, X.; Gao, W.; Yu, J.; An, Q.; Zhang, M.; Hu, Z.; Wang, J.; Tang, W.; Yang, C.; Zhang, F. Ternary Nonfullerene Polymer Solar Cells With Efficiency > 13.7 by Integrating the Advantages of the Materials and Two Binary Cells. *Energy Environ. Sci.* **2018**, *11*, 2134−2141.
(74) Yang, L.; Song, X.; Yu, J.; Wang, H.; Zhang, Z.; Geng, R.; Cao, J.; Baran, D.; Tang, W. Tuning of the Conformation of Asymmetric Nonfullerene Acceptors for Efficient Organic Solar Cells. *J. Mater. Chem. A* **2019**, *7*, 22279−22286.
(75) Song, J.; Li, C.; Zhu, L.; Guo, J.; Xu, J.; Zhang, X.; Weng, K.; Zhang, K.; Min, J.; Hao, X.; Zhang, Y.; Liu, F.; Sun, Y. Ternary Organic Solar Cells with Efficiency > 16.5 Based on Two Compatible Nonfullerene Acceptors. *Adv. Mater.* **2019**, *31*, 1905645.
(76) MacKenzie, R. C. I.; Shuttle, C. G.; Chabinyc, M. L.; Nelson, J. Extracting Microscopic Device Parameters from Transient Photocurrent Measurements for P3HT:PCBM Solar Cells. *Adv. Energy Mater.* **2012**, *2*, 662.
(77) Huang, J. S.; Goh, T.; Li, X.; Sfeir, M. Y.; Bielinski, E. A.; Tomasulo, S.; Lee, M. L.; Hazari, N.; Taylor, A. D. Polymer Bulk Heterojunction Solar Cells Employing Forster Resonance Energy Transfer. *Nat. Photonics* **2013**, *7*, 479−485.
(78) Lv, R.; Chen, D.; Liao, X.; Chen, L.; Chen, Y. A Terminally Tetrafluorinated Nonfullerene Acceptor for Well Performing Ally Ternary Solar Cells. *Adv. Funct. Mater.* **2019**, *29*, 1805872.

https://doi.org/10.1021/acsomega.2c05141
ACS Omega 2023, 8, 1989−2000